Geomorphology 377 (2021) 107582

Contents lists available at ScienceDirect

Geomorphology

journal homepage: www.elsevier.com/locate/geomorph

Networks of unusually large fossil periglacial polygons, Campine area, northern Belgium

Koen Beerten [a,*], Erwin Meylemans [b], Cornelis Kasse [c], Thomas Mestdagh [d,e], David Van Rooij [d], Jan Bastiaens [b]

[a] Engineered and Geosystems Analysis, Belgian Nuclear Research Centre, SCK•CEN, Mol, Belgium
[b] Flanders Heritage Agency, Brussels, Belgium
[c] VU University Amsterdam, Department of Earth Sciences, Amsterdam, the Netherlands
[d] Renard Centre of Marine Geology, Department of Geology, Ghent University, Ghent, Belgium
[e] Flanders Marine Institute (VLIZ), Ostend, Belgium

ARTICLE INFO

Article history:
Received 4 September 2020
Received in revised form 16 December 2020
Accepted 17 December 2020
Available online xxxx

Keywords:
LiDAR DEM
Thermal contraction cracking
Polygon networks
Weichselian permafrost

ABSTRACT

A series of polygon networks has been discovered on the most recent LiDAR (Light Detection and Ranging) DEM (Digital Elevation Model) of Flanders (Belgium) available in a resolution of 1 m^2. They are located in the sandy Campine area (northern Belgium) and resemble thermal contraction crack polygon networks from present-day permafrost regions. Different network types were observed, ranging from orthogonal to hexagonal and various combinations of these. The inter-polygon troughs are typically several decimeters deep and up to several meters wide. The average polygon size is ca. 3000 m^2, which is equivalent to a diameter of ca. 60 m if the polygon shape is approximated with a perfect circle, or a side of ca. 55 m length if it were to be approximated by a perfect square. The average size is (much) larger than any of the studied present-day analogues, and also larger than fossil networks in the western part of Flanders, Poland and France. In contrast to the Campine polygons presented here, the fossil analogues in these countries were detected using satellite imagery and orthophotos, which may partially explain the observed size differences. The morphometric analysis of the Campine networks shows relationships between polygon type and local geomorphological position as orthogonal networks seem to have a preference to develop near shallow valley slopes. In addition, GPR (Ground Penetrating Radar) radargrams were acquired across polygon boundaries to investigate subsoil disturbances related to the former position of ice wedges or sand wedges. However, the evidence is not unequivocal due to the low dielectric contrast between the host and wedge material. It is not clear yet whether smaller 2nd and 3rd order cracks did develop but without leaving a topographical imprint. The observed polygon networks in the Campine area are interpreted as first-order networks that developed during a time span of several thousands of years, up to 10 kyr at most, in a former Late Weichselian permafrost climate.

1. Introduction

Present-day lowland permafrost regions around the world have a set of characteristic landscape features that are unique to the environment which they are being formed in. One such particular feature is the presence of patterned ground, in the form of polygonal networks. They are thought to be the result of thermal contraction cracking of the soil, under cold climatic conditions and strong vertical temperature gradients in the upper part of the soil (e.g., Lachenbruch, 1962). The thermal contraction cracks tend to organize themselves into a polygonal network, the shape and dimensions of which are supposed to be dependent on (sub)soil characteristics, the local geomorphology, soil moisture, vegetation, temperature gradient, mean annual temperature and duration of permafrost conditions (see, e.g., Ulrich et al. (2011)).

Many polygon networks have been observed on aerial photographs from regions that are located outside the present permafrost boundaries, which is seen as evidence for these regions to have once experienced cold climate conditions with permafrost development. Such networks have for instance been identified in the Netherlands (de Gans, 1983), Poland (Ewertowski et al., 2017), France (Bertran et al., 2013; Andrieux et al., 2016) and Belgium (Ghysels and Heyse, 2006; Ghysels, 2008). The polygons are usually preserved as cropmarks (or, more in general, vegetation marks in the case of grassland), and often their traces are vague, time transient and dependent on weather conditions. Arctic analogues are known to be visible on detailed digital elevation models (DEM), because the crack is usually marked as a weak topographic low in the landscape. Remarkably, similar structures have been observed on recent LiDAR (Light Detection and Ranging) images

* Corresponding author.
E-mail address: kbeerten@sckcen.be (K. Beerten).

https://doi.org/10.1016/j.geomorph.2020.107582
0169-555X/

of the Campine area, NE Belgium. The presence of past permafrost conditions in northwestern Europe, including the Campine area, has already been evidenced by numerous observations of ice-wedge casts and relict sand wedges in geological outcrops, that are interpreted as fossil thermal contraction cracks (Gullentops et al., 1981; Vandenberghe, 1983; Vandenberghe and Pissart, 1993; Ghysels and Heyse, 2006; Kasse et al., 2007).

Relict periglacial features have been used in the past for the reconstruction of the former distribution and characteristics of permafrost, in the context of palaeoclimatological research (e.g., Ballantyne and Harris, 1994). These features include, amongst others, near-surface cryogenic structures in unconsolidated sediments (e.g., ice-wedge casts, sand wedges, polygons, cryoturbations), mass-wasting landforms and structures (e.g., solifluction sheets and lobes), and aeolian and niveo-aeolian features (e.g., sand dunes). However, a number of researchers have urged caution over the use of this type of evidence as present-day Arctic areas are not necessarily good analogues for the periglacial regimes that prevailed in the mid-latitudes during former cold stages, since the latter would have experienced quite different solar radiation cycles from those that prevail at the poles today (Lowe and Walker, 1997). The overall objective of this study is to frame the newly discovered polygon networks in the Campine area within the present-day knowledge on past periglacial environments and palaeoclimate of the mid-latitudes (lowland Europe). Firstly, the observed networks will be mapped and quantified in terms of shape and dimensions in order to trace internal systematics with respect to local conditions such as subsoil and topographical variations. Secondly, the significance of LiDAR DEM observed networks will be explored by comparing them to vegetation marks and GPR (Ground Penetrating Radar) images, whenever available, and present-day and fossil analogues. Finally, this would allow us to formulate several meaningful characteristics of former permafrost conditions in the Campine area, and how they governed the development of the polygon networks.

2. Regional setting

The study area is located in the Campine region, a sandy region in the European Sand Belt, which covers part of northern Belgium and the southern Netherlands (Fig. 1). The Campine region belongs to the geological Campine Basin, a subsiding area which takes an intermediate position in between the uplifting Brabant and Ardennes Massifs to the south, and the rapidly subsiding Roer Valley Graben to the northeast. Continued subsidence caused the Campine Basin to fill with several hundreds of meters of Neogene sediment, mainly sand with some clayey intervals. During the last 0.5 Ma, and perhaps even earlier, the region was exposed to large-scale denudation and erosion (Beerten et al., 2020; Fig. 2a).

The Late Pleistocene subcrop map (Fig. 2b) shows the distribution of the main Plio-Pleistocene sediments in the region, excluding local aeolian and fluvial deposits (H3O – De Kempen; Vernes et al., 2018). In general, the sediments are sandy with several sparse and thin peat beds, especially in the Pliocene Mol Formation, and in the Early Pleistocene Malle Formation and Stramproy Formation. The Early Pleistocene Weelde Formation contains several distinct clay layers reaching a thickness of several meters. Finally, the Early to Middle Pleistocene Sterksel Formation is a Rhine deposit consisting of coarse sand with some gravel, reaching a thickness of several meters. All formations gently dip and become younger towards the north. Mostly, the formations mentioned above are covered with a thin layer of Late Pleistocene to Holocene sand, mostly aeolian and sometimes building up a dune relief, and fluvial deposits in the river valleys, consisting of a mixture of sand, silt, clay and peat. As a result of these shallow sandy cover layers, the dominant soil texture in the region is sand, according to the Belgian soil classification system (Geopunt, 2017).

The clayey Weelde Formation is responsible for the existence of a cuesta in the region, the so-called Campine Clay cuesta (Fig. 2a). It forms a positive relief, relative to the area south (belonging to the Scheldt catchment) and north (belonging to the Meuse catchment) of it, due to its larger erosion resistance compared with the unconsolidated fine sands of the underlying and overlying formations. The southern limit of the Weelde Formation marks the edge of the cuesta (compare Figs. 1, 2a and b) as well as the southernmost extent of a relatively shallow clay layer in the subsurface. Note that the Weelde Formation continues to the north of its Late Pleistocene subcrop area, underneath the Stramproy and Sterksel Formations.

The reconstructed Weichselian palaeotemperature curve for Flanders is given in Fig. 3 (Govaerts et al., 2016). The curve was initially constructed for Weichselian permafrost depth calculations in the Netherlands (bordering Flanders) but used here as an approximation for the last glacial temperature history of Flanders. Estimates for the mean annual air temperature (MAAT) during MIS5 (marine isotope stage 5) are based on pollen data from van Gijssel (1995), but replotted against a more recent chronostratigraphical framework for the Weichselian glaciation (see e.g., Busschers et al., 2007). The main features of the MIS5 climate are the relatively cold stadials 5b and 5d, with an MAAT of −2 °C, and the relatively mild interstadials 5c and 5a, with an MAAT of +4 °C. The first period with continuous permafrost development in Flanders would have been MIS4, with MAAT values dropping to as low as −4 °C and even −8 °C for the end of MIS4. These values are based on periglacial deformation phenomena (e.g., ice-wedge casts and large-scale involutions) in the shallow subsoil and their present-day distribution in areas of stable

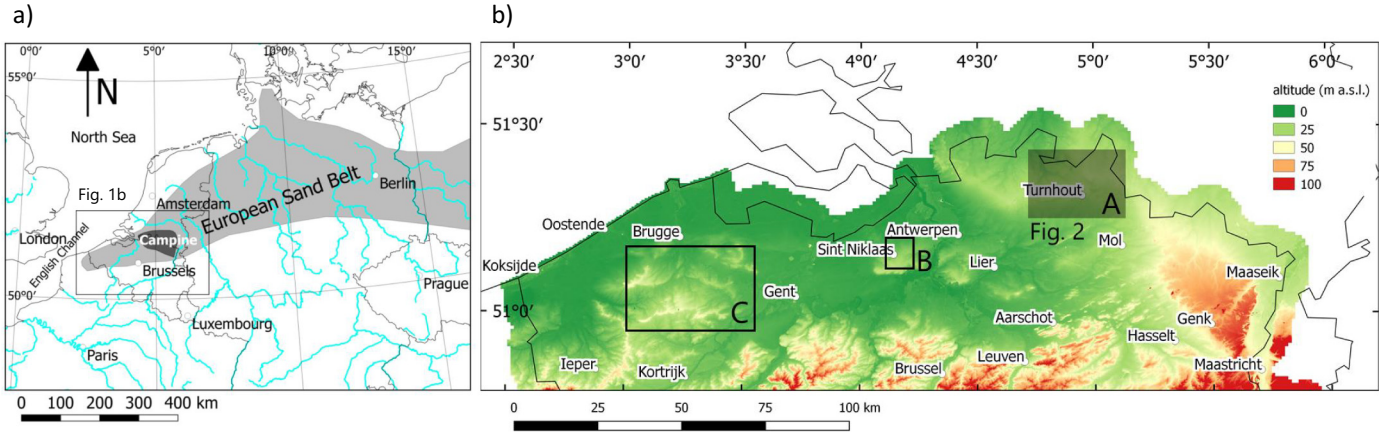

Fig. 1. (a) General location of the Campine region in western Europe. (b) Digital Elevation Model (DEM) of Flanders (AGIV, 2014), showing the areas of interest mentioned in the text. A: study area (Campine Clay cuesta), B: Land van Waas (Boom Clay cuesta), C: Central Western-Flanders hilly region.

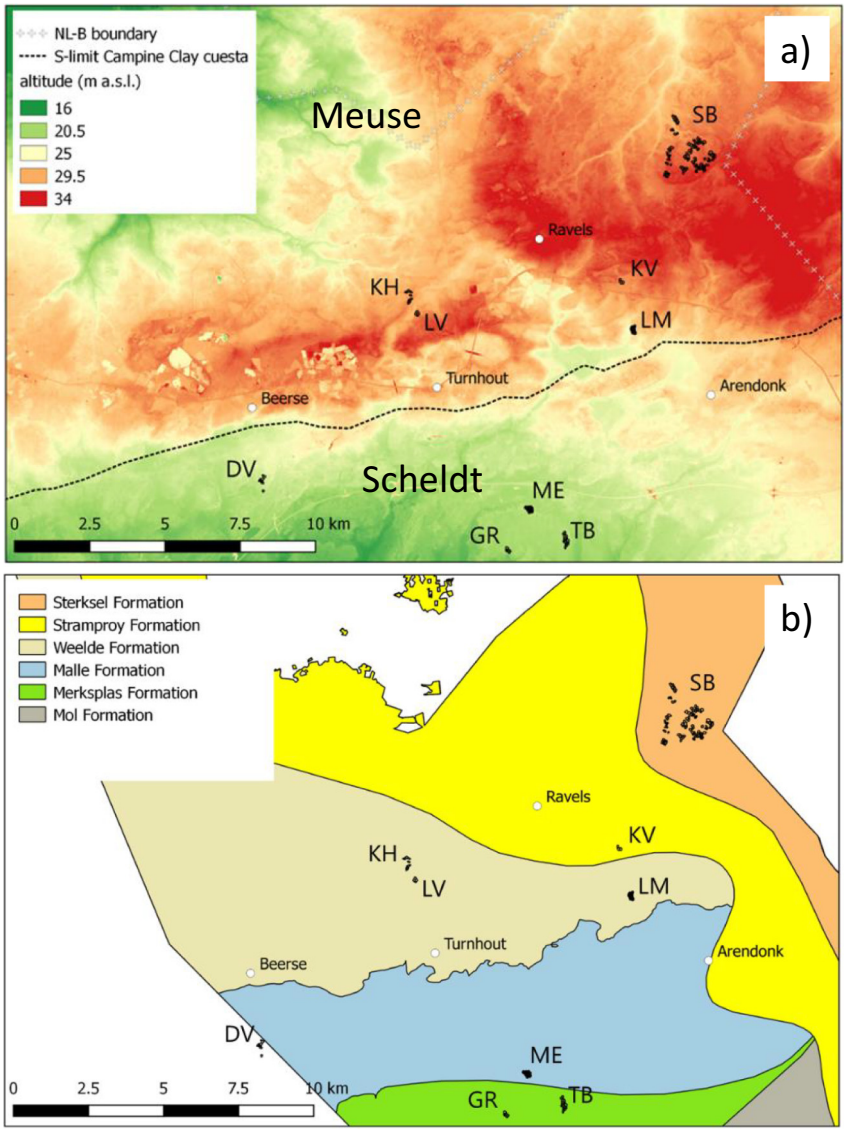

Fig. 2. (a) Distribution of mapped polygons in the Campine area against the DEM. The sites are abbreviated as follows: SB = Staatsbossen Ravels, KV = Kijkverdriet Ravels, LM = Liereman Oud-Turnhout, KH = Koevenheide Turnhout, LV = Langvenstraat Turnhout, DV = Dekkersven Vosselaar, ME = Mellen Turnhout, GR = Grote Reesdijk Turnhout, TB = Tikkebroeken Kasterlee. The dotted line indicates the southern boundary of the clay-rich Weelde Formation, and coincides morphologically with the boundary between the Campine Clay cuesta in the north, and the sandy Brasschaat Pediment in the south. (b) Distribution of mapped polygon nets in relation to the geology of the study area (Vernes et al., 2018). The Weelde Formation contains several distinct estuarine clay layers and dips towards the north underneath the fluvial Stramproy and Sterksel Formations. The dominant lithology in the Sterksel, Stramproy, Malle, Merksplas and Mol Formations is fine to coarse sand. (For interpretation of the references to color in this figure legend, the reader is referred to the web version of this article.)

continuous permafrost (Vandenberghe and Pissart, 1993; Huijzer and Vandenberghe, 1998; Vandenberghe et al., 2014). The following MIS3 is characterised by a somewhat milder climate, showing less periglacial deformation of the subsoil. Analysis of flora and fauna preserved within MIS3 sediments, and the type and nature of periglacial deformation shows that some interstadials might have reached an MAAT between 0 °C and +6 °C (e.g., Upton Warren, Hengelo and Denekamp interstadials; Huijzer and Vandenberghe, 1998, Busschers et al., 2007 and van Gijssel, 1995), and several stadials would have reached an MAAT as low as −4 °C (e.g., Hasselo stadial; Busschers et al., 2007). Subsequently, the climate evolves towards the Late Glacial Maximum (LGM), which is situated in MIS2. Data for this stage is mainly derived from Renssen and Vandenberghe (2003) and Buylaert et al. (2009), and is based on the presence and type of periglacial deformation phenomena. The MAAT for the period between 28 ka and 15 ka would not have exceeded 0 °C, while some periods show MAAT values as low as −8 °C. The end of MIS2 is characterised by stepwise global warming, showing significant variations between interstadials (Alleröd-Bølling) and stadials (Younger Dryas). Finally, present-day MAAT values of around +10 °C are attributed to MIS1. In general, the period around the LGM (ca. 20 ka) is thought to have been characterised by severe aridity, as well as the following millennia, until the start of the Late Glacial around 15 ka BP (Kasse, 2002).

As can be seen from Fig. 3, suitable time windows for the development of thermal contraction crack polygons are not very numerous and rather short. For sandy soils to crack in discontinuous permafrost, an MAAT of −3/4 °C or less is needed, and cracking in continuous permafrost would need an MAAT below −8/9 °C (see references in Section 2). The latter condition is only met during MIS4 and MIS2, for a duration of around 5 kyr.

3. Formation mechanism of contraction crack polygons

The development of thermal contraction cracks can be ascribed to the repeated freezing and thawing of the soil in areas with a cold climate

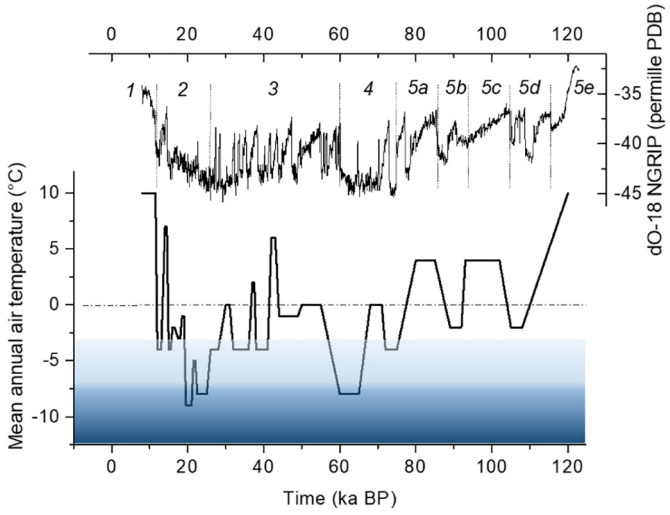

Fig. 3. Best estimate temperature evolution for the Weichselian glaciation in Flanders (Govaerts et al., 2016). Pale shading refers to the temperature interval where continuous permafrost may be expected in fine-grained material (clay, silt) and discontinuous permafrost in coarse-grained material (sand, gravel), while dark shading indicates the interval where continuous permafrost may be expected in coarse-grained material as well. The curve is based on data from van Gijssel (1995), Huijzer and Vandenberghe (1998), Renssen and Vandenberghe (2003), Busschers et al. (2007) and Buylaert et al. (2009). Marine isotope stages (numbering 1 to 5e) are taken from Busschers et al. (2007) and references therein. The oxygen isotope curve is reproduced from NGRIP (2004) data.

that experience permafrost or deep seasonal frost (Lachenbruch, 1962). In winter, the soil freezes completely and a thin crack is formed by thermal contraction. During the next summer and early autumn, when the upper part of the soil is thawed (the active layer), water is seeping through the crack into the frozen soil below the active layer and freezes. In permafrost regions, this process may be repeated several 100 times, such that an ice wedge is formed. Thermal contraction cracks organize themselves into a network. A physical explanation for the mechanics of the evolution of these cracks was first proposed by Lachenbruch (1962). A necessary condition for soil to crack under thermal loading (contraction) is an episode of large temperature gradients in the upper soil (active layer) above the permafrost table, as a result of a sudden air temperature drop (French, 2007). The mean annual air temperature (MAAT) at which cracking would occur has been estimated to be $<-3/4$ °C for clay, silt and peat and $<-6/8$ °C for sand and gravel (Romanovskii, 1985; Vandenberghe and Pissart, 1993; Ballantyne and Harris, 1994). The unique relationship between ice-wedge formation and MAAT has been criticized by, a.o., Murton and Kolstrup (2003) who argue that fossil ice-wedges in general can be used to infer past permafrost only, and not the severity of the permafrost (ground temperature), and by Plug and Werner (2001) who argue that wedge spacing and width in ice-wedge networks mainly reflect infrequent episodes of rapidly falling ground temperatures rather than mean conditions. Indeed, amongst others, insulation by snow and/or vegetation may alter the atmosphere-soil coupling and reduce the accumulation of thermal stress, thus limiting continuous frost cracking (French, 2007; Kokelj et al., 2007). The initial polygon size is believed to depend mainly on two parameters, namely the temperature gradient in the upper soil and the rheology of the frozen ground. In theory, larger temperature gradients will lead to more cracks and thus smaller polygon size (French, 2007). Furthermore, the coefficient of thermal expansion plays a major role since it is much larger for ice-rich fine-grained material than for ice-poor coarse-grained material. As a result, polygons are generally smaller in ice-rich clay soils (Lachenbruch, 1962, 1966). With regard to polygon form, the stage of development seems to be an important governing factor. According to Lachenbruch (1966), French (2007) and Haltigin et al. (2012) polygon networks tend to become more regular and the polygon intersections more rectangular with time. Consequently, secondary and even tertiary cracks form, leading to the subdivision of existing polygons. As a result, the final polygon size, as seen in the field, will be smaller. Anisotropy such as systematic topography and horizontal stress differences (e.g., a bordering escarpment) usually favours the formation of oriented and orthogonal networks, while uniform cooling of a homogeneous soil promotes the development of hexagonal networks (Lachenbruch, 1962; French, 2007).

Sletten et al. (2003) on the other hand hypothesize another evolutionary path for thermal contraction crack polygons, based on field work in the Dry Valley of Antarctica. According to their interpretation, young polygon nets are large and often orthogonal, which they describe as the initiation phase. With time, they evolve into a network of more evenly spaced orthogonal and non-orthogonal cracks subdividing the large polygons; this is the developmental phase. Finally, mature polygons are regular with non-orthogonal cracks. This evolution scheme is slightly different from the one that Haltigin et al. (2012) and Ulrich et al. (2011) put forward, suggesting that polygons become more orthogonal with age.

4. Materials and methods

Polygon networks were identified on the LiDAR-derived DEM of the Campine area (AGIV, 2014), and some of them were verified in the field. Subsequently these networks were digitized using QGIS software, which resulted in a series of shapefiles. Only the best visible parts of the polygon networks have been mapped, the total network may often be broader. The networks were then qualitatively classified according to the scheme of French (2007): orthogonal, random orthogonal, random mixed, random hexagonal, hexagonal. Next, polygon size parameters (mean area (MEAN), median, standard deviation (STD), minima and maxima) and the percentage of orthogonal (ORTHO) and 4-ray intersections (i.e., a junction of 4 polygon boundaries; 4RAY) were quantified for various polygon networks (QGIS). As indicated above, these metrics are informative about the initial conditions and evolution of polygon networks.

As to understand the inter-network polygon variation due to differences in substrate and/or soil characteristics, the obtained metrics were tested against subsurface parameters from the digital soil map of Flanders (Geopunt, 2017) and various geological models (Geopunt, 2013; Vernes et al., 2018). Finally, network characteristics were compared with present-day and Late Pleistocene analogues from the northern hemisphere, as found in the literature. Note that these are based on airborne imagery, not detailed DEM images.

Subsurface information was acquired using Ground Penetrating Radar (GPR). This survey deployed a Mala GPR-system with ProEx control unit. A 250 MHz shielded antenna (mounted on a rough terrain cart, profile 257) and 100 MHz shielded antenna (in towing mode, profiles 291–301) were used. Within the soil conditions of this study, the 250 MHz antenna yields a resolution of 10–15 cm and penetration depth of $\pm$2–3 m, while the 100 MHz gives a lower resolution ($\pm$30 cm) but deeper penetration (up to $\pm$6 m). The sampling interval along the profiles was 4 cm for profile 257, and 5 cm for profiles 291–301. XY-coordinates of the sampling points were recorded by connecting a GPS-device to the control unit of the GPR. Post-processing was performed in RadExplorer, and included DC offset removal, amplitude correction (for spherical divergence) and bandpass filtering. Estimates of the electromagnetic wave propagation velocity in the subsurface (in the range of 5.4–6.3 cm/ns) were obtained for the study area by fitting theoretic hyperbolas to observed diffraction hyperbolas in the data. This allows to convert the depth scale in which the data was acquired (i.e. nanoseconds two-way travel time) to depth in meters. Each profile was corrected for topographical variations, using a modelled depth-width relationship for the troughs delineating the polygons, based on the LiDAR images.

Although there are limitations to using them as present-day analogues, exploring current polygon networks in Arctic (and Antarctic)

regions and comparing their characteristics with fossil ones may yield at least some supplementary information on the initial conditions, the subsequent development and the palaeoenvironmental context of the observed fossil networks. The analogues are situated in the northern hemisphere (Canada, Alaska and Norway), roughly between 60 and 80°N (Table 1). Their selection is primarily based on the availability and accessibility of data on various polygon parameters, and if not available from the published study, the possibility to derive them from the digitalization of accompanying maps. The analogues in Table 1 are ranked according to the present-day MAAT at the site. Although they cover a wide range of MAAT values and are found in various different latitudes, the analogue sites have a few characteristics in common. They are usually located near the coast, at a low altitude, in a sparsely vegetated environment mostly on loose granular sedimentary soil. They are obviously located in regions that are experiencing continuous permafrost, in a cold climate with low precipitation values (usually below 300 mm/year) and a MAAT between −6 °C and −16 °C. The time window for polygon formation is derived from the local deglaciation, uplift and/or incision histories of the sites. The sites with the lowest MAAT (−15 °C) are located in northern Canada, along the Arctic coast, at latitudes between 75 and 80°N (Devon Island and Axel Heiberg Island). The latter has seen a rather short time window for network development, i.e., 2.5 kyr. Two sites near the northern Alaskan coast (Barrow and Prudhoe Bay) have MAAT values of ca. −11 °C, yet their deglaciation history started before 12 ka BP. The same deglaciation history is valid for the two sites along the northern Canadian coast in the Northwestern Territories (upland and lowland sites at Garry and Richards Island located at ca. 69°N), while their present-day MAAT is around −7.5 °C. The most continental sites of the North American analogues are the ones located along the Sugluk inlet, and actually consist of a series of polygon networks that developed on fluvial terraces at different altitudes. Even though it is located in a coastal setting, it is to a larger degree surrounded by landmass than the other North American sites. They are located relatively far from the northpole (ca. 62°N). The time window for polygon development decreases from 5 kyr for the uppermost terrace to 3.5 kyr for the lowermost terrace. The European sites are all located on Svalbard, in the Arctic Ocean, in the Adventdalen region. Although their latitudinal position is at ca. 78°N, the present-day MAAT is relatively high compared to the North American sites at similar latitudes, i.e., ca. −6 °C. For these sites, the time window for polygon network development is based on the deglaciation history (Farnsworth et al., 2020) and the Holocene relative sea-level history (Long et al., 2012) of Svalbard. For the lowest site (AD1), at ca. 10 m above sea level (a.s.l.), a window of <7 kyr is determined, while for the other three sites (AD2-3-4), at altitudes between ca. 80 m and 170 m a.s.l. a maximum time window of 10.5 kyr is determined.

Two fossil analogues were also included in the morphometric analysis, according to data availability, and their proximity to the Campine area (Table 1). One analogue is in fact a summary of studied polygon networks in France (Andrieux et al., 2016), and one is from the western part of Flanders, only 50–100 km to the west of the Campine area (Ghysels, 2008; see Fig. 1b, rectangles B and C). Both fossil analogues are (Late) Weichselian in age and developed in a permafrost climate.

5. Results

5.1. Polygon metrics from present-day analogues in permafrost regions and fossil analogues in former permafrost regions

The geomorphometric information obtained from present-day and fossil analogues is summarized in Tables 1 and 2. The individual networks

Table 1
Location of the polygon networks that were studied as a potential analogue (present-day and fossil), their location, latitude, altitude (m a.s.l.), mean annual air temperature (MAAT), mean annual precipitation (P), soil characteristics, geomorphological setting, vegetation, time window for development of the networks and the corresponding reference (n/d = not determined; n/a = not applicable). For comparison, a summary of the Campine data is also included.

Site	Location	Coordinates	Altitude (m)	MAAT (°C)	P (mm/year)	Soil characteristics	Local geomorphology	Vegetation	Duration (kyr)	Reference
Devon Island	Nunavut, Canadian Arctic coast	75°N 87°W	35	−16	180	Fine grained floodplain + carbonate silts	Floodplain	None	7.5	Haltigin et al. (2012)
Axel Heiberg Island	Nunavut, Canadian Arctic coast	79°N 91°W	18	−15	100	Fine and coarse floodplain	Alluvial fan	None	2.5	Haltigin et al. (2012)
Barrow	Northern Alaskan Arctic coast, USA	71°N 156°W	7	−11	115	Sand, gravel and silt	Coastal plain	Tundra	>12	Dafflon et al. (2016)
Prudhoe Bay	Northern Alaskan Arctic coast, USA	70°N 148°W	75	−11	77	Alluvial sand and gravel	Lowland plain	Tundra	>12	Abolt et al. (2017)
Sugluk Inlet, D4	Hudson Bay, Canada	62°N 75°W	33	−8	310	Sand and peat	River terrace	Tundra/shrubs	5	Kasper and Allard (2001)
Sugluk Inlet, D1	Hudson Bay, Canada	62°N 75°W	12	−8	310	Sand and peat	River terrace	Tundra/shrubs	4.5	Kasper and Allard (2001)
Sugluk Inlet, G5	Hudson Bay, Canada	62°N 75°W	5	−8	310	Sand and peat	River terrace	Tundra/shrubs	3.5	Kasper and Allard (2001)
Garry and Richards Island upland	NW Territories, Canadian Arctic coast	69°N 134°W	16	−7.5	179	Sand and silt	Upland	Tundra	>12	Burn and O'Neill (2015)
Garry and Richards Island lowland	NW Territories, Canadian Arctic coast	69°N 134°W	4	−7.5	179	Sand and silt	Lowland	Tundra	>12	Burn and O'Neill (2015)
Adventdalen AD1	Svalbard, Norway	78°N 16°E	10	−6	180	Silt (aeolian loam)	Glacial valley	Closed tundra/shrubs	3	Ulrich et al. (2011)
Adventdalen AD2	Svalbard, Norway	78°N 16°E	80	−6	180	Glaciofluvial sediment, including gravel	Glacial valley	Closed tundra/shrubs	<7	Ulrich et al. (2011)
Adventdalen AD3	Svalbard, Norway	78°N 16°E	80	−6	180	Solifluction material and weathered bedrock	Glacial valley	Closed tundra/shrubs	<7	Ulrich et al. (2011)
Adventdalen AD4	Svalbard, Norway	78°N 16°E	140	−6	180	Weathered bedrock	Glacial valley	Closed to open tundra/shrubs	<7	Ulrich et al. (2011)
West Flanders	Belgium	51°N 3°E	n/a	n/a	n/a	(Silty) sand to clay	Hilly interfluve	n/a	n/d	Ghysels (2008)
France	France	44–50°N	n/d	n/a	n/a	Mixed soil types	n/d	n/a	n/d	Andrieux et al. (2016)
Campine	Belgium	51°N 5°E	20–30	n/a	n/a	Sand, occasionally underlain by shallow clay substrate	Cuesta/pediment	n/d	n/d	This study

Table 2
Metrics of the analogue networks (present-day and fossil): number of polygons (N), mean area (MEAN), median area (MEDIAN), relative standard deviation (RSD), minimum area (MIN), maximum area (MAX), total number of counted intersections (N_i), percentage of 4-ray intersections (4RAY), and percentage of orthogonal intersections (ORTHO) (n/d = not determined; n/a = not applicable). For comparison, a summary of the Campine data is also included.

Site	Polygon type	N	MEAN (m^2)	MEDIAN (m^2)	RSD (%)	MIN (m^2)	MAX (m^2)	N_i	4RAY (% 4-ray inter-sections)	ORTHO (% orthogonal intersections)
Devon Island	Oriented orthogonal	93	397	386	38	119	836	112	55	97
Axel Heiberg Island	Random orthogonal	78	153	130	62	20	580	117	13	32
Barrow	Irregular mixed	135	310	274	57	93	1049	112	12	65
Prudhoe Bay	Random orthogonal	9	204	198	24	121	291	50	28	74
Sugluk Inlet, Hudson Bay, D4	Random orthogonal	17	80	59	63	30	191	33	21	79
Sugluk Inlet, Hudson Bay, D1	Random orthogonal	22	150	131	53	33	329	23	30	78
Sugluk Inlet, Hudson Bay, G5	Random orthogonal	17	173	124	83	8	504	26	11	69
Garry and Richards Island upland	Random ortho/hexagonal	21	743	723	63	214	1764	27	26	63
Garry and Richards Island lowland	Random ortho/hexagonal	53	373	307	52	166	1093	83	15	66
Svalbard Adventdalen AD1	Pentagonal, hexagonal	185	340	268	77	51	2029	n/a	10	n/a
Svalbard Adventdalen AD2	Pentagonal, hexagonal	241	771	594	69	70	3329	n/a	4	n/a
Svalbard Adventdalen AD3	Pentagonal, hexagonal	103	559	447	68	85	2101	n/a	7	n/a
Svalbard Adventdalen AD4	Hexagonal on dry terrace and orthogonal down the slope	159	507	83	65	75	1786	n/a	9	n/a
West Flanders	Mixed	145	104	58	112	4	760	178	18	46
France	n/d	n/d	179	n/d	n/d	63	380	n/a	n/a	n/a
Campine	Mixed	210	3128	2912	54	454	9401	243	20	31

are characterised by a wide range of sizes, polygon classes and anticipated ages. For instance, polygon sizes on different terrace levels along the Sugluk Inlet (Hudson Bay, NE Canada; Kasper and Allard, 2001) seem to be rather small (100–200 m^2) in comparison with those observed in the uplands of Garry and Richards Island in NW Canada (750 m^2; Burn and O'Neill, 2015) and Adventdalen in Svalbard, Norway (400–800 m^2; Ulrich et al., 2011) (Table 2). The various Sugluk Inlet networks show internal consistency. The oldest ones (on the highest terrace levels) have the smallest polygons and the largest amount of orthogonal and 4-ray intersections, in line with the theory that individual polygons become smaller and more organized with time. Well organized networks are observed in northern Canada (Devon Island), where the proportion of orthogonal intersections in polygons that developed during a time period of 7.5 kyr is almost 100%, while this is only 32% for polygon networks that only developed during a time period of 2.5 kyr (Axel Heiberg Island; Haltigin et al., 2012). Here, the effect of initial conditions or other factors than time is clearly illustrated by the fact that the Axel Heiberg polygons are smaller than the Devon Island polygons, while the opposite would be expected according to their age. The influence of local conditions can also be seen in NW Canada, where polygons in the lowlands of Garry and Richards Island are much smaller than those of the adjacent uplands, which is attributed to the high water content of the lowland terrain (in comparison with the well-drained 'upland'). Note that these networks have been developing for >12 kyr, as is the case for those at Prudhoe Bay (Abolt et al., 2017) and Barrow (Dafflon et al., 2016) near the Beaufort Sea, Northern Alaska (USA). Yet, the percentage of orthogonal intersections is around 65%, which indicates that time is not the only factor determining the shape and size of polygon networks. Rather immature polygon networks are found in Svalbard, where various networks along the Adventdalen show a low percentage of 4-ray intersections (orthogonal intersections were not included in that study). The Adventdalen polygons are amongst the largest in the otherwise rather small data set of present-day analogues (up to almost 800 m^2 on average for AD2, the largest individual polygon being larger than 3000 m^2). The youngest Adventdalen network (AD1) is mainly orthogonal with the smallest individual polygons, while the older ones are hexagonal and pentagonal with larger polygons. This is explained by the fact that cracking in AD2-3-4 stopped and ice-wedges became inactive (Ulrich et al., 2011).

Fossil analogues are those that are found in regions outside the present-day permafrost realm (Tables 1 and 2). The fossil analogues closest to the Campine study area (NE Belgium) in this work are polygon networks that are found in the western part of Flanders (NW Belgium; Fig. 1b), and have been studied intensively by Ghysels (2008). These polygons were mapped from cropmarks, and some of them were verified in the field using planar- and cross-sections through the associated ice-wedge casts and sand-wedge relicts. On average, the individual polygons are rather small, ca. 100 m^2 on average, ranging between 4 m^2 and 760 m^2. The percentage orthogonal intersections is ca. 50%. The associated wedge casts, some of which are very small (only up to several dm wide), can be subdivided into sand wedges on the interfluves and composite wedges (mixed ice and sand) in depressions (Ghysels and Heyse, 2006). Optically stimulated luminescence (OSL) ages of sediment in the wedges range between 22 ka and 14 ka. In France, relict polygons have been mapped by Andrieux et al. (2016), based on cropmarks. The study does not provide metrics on individual networks, but the overall mean individual polygon size for the whole of France is ca. 180 m^2 (recalculated from an average polygon diameter of ca. 15 m, assuming a circular shape), ranging between 63 m^2 and 380 m^2. They are believed to be Late Weichselian in age and developed on a wide variety of soils and substrates. Some networks, notably those that developed in gravel-rich soil, typically have larger polygons (Bertran et al., 2013). In Poland polygons have been studied by Ewertowski et al. (2017) based on cropmarks. The authors also attributed them to thermal contraction crack polygons and specified 6 types: (A) nets of large and irregular orthogonal polygons, (B) complex small irregular orthogonal polygons, (C) regular orthogonal polygons, (D) irregular non-orthogonal polygons, (E) regular non-orthogonal polygons and (F) mixed orthogonal and non-orthogonal polygons. Their hypothesis, i.e., that polygon nets would show aging features towards the south (being deglaciated earlier due to the northward retreat of the Weichselian ice sheet), could not be confirmed. The few OSL ages they obtained from related ice/sand-wedge casts range roughly between 18 ka and 14 ka. The authors did not include a quantitative analysis of polygon metrics, yet it is clear that a wide range of polygon types and sizes exists in a relatively small area (2000 km^2). Some networks have polygon sizes up to ca. 2500 m^2 (type A, based on their Fig. 6a), and others show networks of very large orthogonal polygons with higher order and less well developed non-orthogonal subdivisions (type F, based on their Fig. 8b).

5.2. Contraction crack polygon networks observed on the LiDAR-based DEM of the Campine area

5.2.1. Description of the polygon networks

Study of the LiDAR images revealed many sites with potential polygons in the Campine area. Nine have been studied more in detail, as they show the clearest polygon networks. The location and distribution of these polygons is given in Fig. 2a and Table 3. All relevant parameters of the various polygon networks are summarized in Table 4.

Table 3
ID of the mapped Campine polygon networks, the name of the site, the municipality they were found in, the corresponding (approximate) Lambert coordinates and the average altitude (m a.s.l.). Also given are the geomorphological, pedological, hydrological and geological context of the mapped polygons. The geomorphological unit within Belgium refers to De Moor and Pissart (1992). Soil texture and drainage class are derived from the soil map of Flanders (Geopunt, 2017).

ID	Site name	Town	X (m)	Y (m)	Z (m)	Geomorphological position within Flanders	Local geomorphological position of the site	Geology below 2 m depth (Formation)	Depth to clay (m)	Surficial geology (Formation)	Soil Texture	Current drainage class
SB-1	Staatsbossen	Ravels	197,250	233,207	30.5	Campine Clay cuesta	Smooth valley border	Weelde	5 to 10	Gent-Sterksel-Stramproy	Z(y)	c–d
SB-2	Staatsbossen	Ravels	197,854	232,313	31.5	Campine Clay cuesta	Undulating valley border	Weelde	>10	Gent-Sterksel-Stramproy	Z(y)	c–d
SB-3	Staatsbossen	Ravels	196,960	231,336	32.5	Campine Clay cuesta	Undulating crest	Weelde	>10	Gent-Sterksel-Stramproy	Z(y)	c–d
KV	Kijkverdriet	Ravels	195,431	227,749	30.5	Campine Clay cuesta	Undulating crest	Weelde	2 to 5	Gent-Stramproy	Z	d–e
KH-1	Koevenheide	Turnhout	188,425	227,507	30	Campine Clay cuesta	Undulating crest	Weelde	2 to 5	Gent	Z(y)	d–e
KH-2	Koevenheide	Turnhout	188,353	227,070	30	Campine Clay cuesta	Undulating crest	Weelde	0 to 2	Gent	Z(y)	d–e
LV	Langvenheide	Turnhout	188,671	226,680	30.5	Campine Clay cuesta	Smooth dipping valley border	Weelde	0 to 2	Gent	Z	d–e
LM	Liereman	Oud-Turnhout	195,882	226,094	27	Campine Clay cuesta	Smooth valley border	Weelde	2 to 5	Gent	Z	d–e
DV	Dekkersven	Vosselaar	183,524	220,858	22.75	Brasschaat pediment	Undulating valley border	Malle	>100	Gent	Z	c–d
ME	Mellen	Turnhout	192,380	220,130	21.5	Brasschaat pediment	Smooth valley border	Malle	>100	Gent	Z	c–d
TB	Tikkebroeken	Kasterlee	193,567	218,963	21.5	Brasschaat pediment	Undulating valley border	Malle	>100	Gent	Z(y)	c–d
GR	Grote Reesdijk	Kasterlee	191,691	218,807	20.5	Brasschaat pediment	Smooth valley border	Merksplas	>100	Gent	Z	c–d

One of the first polygon networks discovered, and one of the most clear ones, is Tikkebroeken (TB). Typically, and this holds for most networks, the polygons are found under forest (Fig. 4a). In general the polygons are very large, with polygon boundaries being spaced apart several tens of meters, even up to 100 m (Fig. 4b). A topographical transect through one of the polygons clearly shows the nature and size of the shallow depressions that delineate the polygons. The troughs can be around 10 m wide and up to 40 cm deep, but smaller examples are present as well (Fig. 4c). Site TB is located at ca. 21.5 m a.s.l. on an undulating terrain bordering a shallow valley floor ca. 1–2 m below (Fig. 5a–b). The network is classified as random mixed, with polygon subdivision being visible, especially near the centre of the network. There is no shallow clay substrate here as the Paleogene Boom Clay is at >100 m depth.

The polygon network at site Liereman (LM) is classified as random hexagonal-orthogonal, and assigned to a smooth (non-dipping) valley border morphology (Fig. 5c–d). The site is located at ca. 27 m a.s.l. with a clay substrate (Weelde Formation) starting at a depth of 2–5 m. Individual polygons are quite large and poorly subdivided. The polygons are preserved under woodland and heathland.

Sites Koevenheide KH-1 and KH-2 are located on a crest, reaching an altitude typically 1–2 m above the surrounding landscape (Fig. 5e–f). Both networks are classified as mixed. Here as well, clay from the Weelde Formation starts at a depth of 2 m, up to 5 m. Individual polygons are quite large and poorly subdivided.

The network at Langvenheide (LV) is located on a smoothly dipping surface, which borders a shallow valley floor rather abruptly over a vertical distance of ca. 1–2 m (Fig. 5e–f). It is classified as a pure orthogonal network with large polygons. The clay substrate is rather shallow at depths between 2 and 5 m.

The site at Grote Reesdijk (GR) is located at ca. 20.5 m a.s.l. on a smooth flat terrain bordering a shallow valley (Fig. 5g–h). The network is classified as random hexagonal-orthogonal, with an apparent orthogonal subdivision of otherwise hexagonal polygons. There is no shallow clay substrate here (Boom Clay is at >100 m depth). Grote Reesdijk (GR) is a site where polygons are preserved under a different cover than forest, i.e., cropland. A clear polygon pattern is observed in the investigated cropfield (Fig. 6a). Polygon boundaries are visible as dark marker lines with variable width. The dark colour may indicate different soil and drainage conditions. Interestingly, all polygon boundaries as observed from the orthophoto are captured by the DEM as well, but not vice versa (Fig. 6b). For this site, the DEM is a more powerful tool than the orthophoto to map the polygon network.

The four remaining networks are shown in the supplementary materials (Fig. S1). Site Staatsbossen (SB) is the site with the most extensive polygon networks mapped in the Campine area so far, though not the most clear ones (Fig. S1a–b). The networks are subdivided into three zones, SB-1, SB-2 and SB-3, mainly on the basis of their local geomorphological and topographical position (Fig. S1c–j). SB-3 is located on a sickle-shaped crest, ca. 1–2 m above the surrounding landscape. SB-2 is geomorphologically positioned on low-laying interfluves that are bordered by shallow valleys, with altitude differences up to 1–2 m. Finally, SB-1 is also located on an interfluve between shallow valleys, but at a lower altitude. Polygons from SB-2 and SB-3 show features of polygon subdivision, while these are completely absent from network SB-1 (Fig. S1c–d). SB-1 is classified as a (regular) orthogonal network while SB-2 and SB-3 are classified as random mixed (with hexagonal and orthogonal intersections) networks. The dominant vegetation at the SB sites is woodland.

At site Kijkverdriet (KV) only three polygons could be observed, located on a small crest, which are classified as hexagonal (Fig. S1k–l). They are preserved under grassland. On the orthophoto weak vegetation marks can be observed at this site, but less clear than those at site GR. The clay substrate occurs at a depth of 2–5 m. Site Dekkersven (DV) is located on an undulating surface bordering a valley, but not as abrupt as the network at Langvenheide (Fig. S1m–n). The polygons are classified as a random network. There is no shallow clay substrate

Table 4
Metrics of the observed polygon networks in the Campine area: number of polygons (N), mean area (MEAN), median area (MEDIAN), relative standard deviation (RSD), minimum area (MIN), maximum area (MAX), number of total number of counted intersections (N_i), percentage of 4-ray intersections (4RAY), and percentage of orthogonal intersections (ORTHO). Polygon type according to French (2007).

ID	Site	Polygon type	N	MEAN (m^2)	MEDIAN (m^2)	RSD (%)	MIN (m^2)	MAX (m^2)	N_i	4RAY (% 4-ray inter-sections)	ORTHO (% orthogonal inter-sections)
SB-1	Staatsbossen	Orthogonal	9	3599	3651	25	1964	4853	13	100	54
SB-2	Staatsbossen	Random mixed	23	3604	3489	58	687	9329	32	0	25
SB-3	Staatsbossen	Random mixed	36	2926	2603	55	718	9401	45	17	11
KV	Kijkverdriet	Hexagonal	3	5486	5603	16	4551	6303	4	0	0
KH-1	Koevenheide	Random orthogonal/hexagonal	5	3583	3362	21	2960	4847	6	0	33
KH-2	Koevenheide	Random mixed	8	1949	1710	45	1002	3453	16	0	31
LV	Langvenheide	Orthogonal	4	4625	5233	28	2654	5378	6	0	100
LM	Liereman	Random hexagonal/orthogonal	12	2527	2798	40	571	4065	22	0	23
DV	Dekkersven	Random orthogonal/hexagonal	10	3174	2598	48	1557	5893	14	67	36
ME	Mellen	Random mixed	11	2766	2586	59	639	6723	15	29	47
TB	Tikkebroeken	Random mixed	20	3093	3071	56	454	6404	40	7	35
GR	Grote Reesdijk	Random hexagonal/orthogonal	8	3422	3857	52	1450	6366	13	20	31
ALL	Campine	Mixed	150	3128	2912	54	454	9401	243	26	31

at this site. Finally, the site at Mellen (ML) is located on a surface bordering a shallow valley floor, and is also classified as random (Fig. S1o–p). Again, there is no shallow clay substrate here.

5.3. Semi-quantitative analysis of polygon metrics

Polygon metrics are indicative of a variety of parameters, including those related to the substrate (geology, geomorphology, hydrology, pedology), climate (soil temperature gradients) and time (stage of development) In order to understand which parameters are significant to the development of the Campine polygons, a qualitative analysis of polygon metrics is performed (Tables 3 and 4). The polygon metrics tested here are the mean polygon area for each network (MEAN), the relative standard deviation of the mean (RSD), the percentage of orthogonal intersections in a network (ORTHO) and the percentage of four-ray intersections (4RAY). The mean polygon area for the entire study region is 3128 (±1675) m^2 (Table 4). The smallest polygons are found at site KH-2 (on average 1949 m^2) and the largest at site KV (on average 5486 m^2). The smallest polygon observed in the entire study area is as small as ca. 450 m^2 (site TB) while the largest is as large as ca. 9400

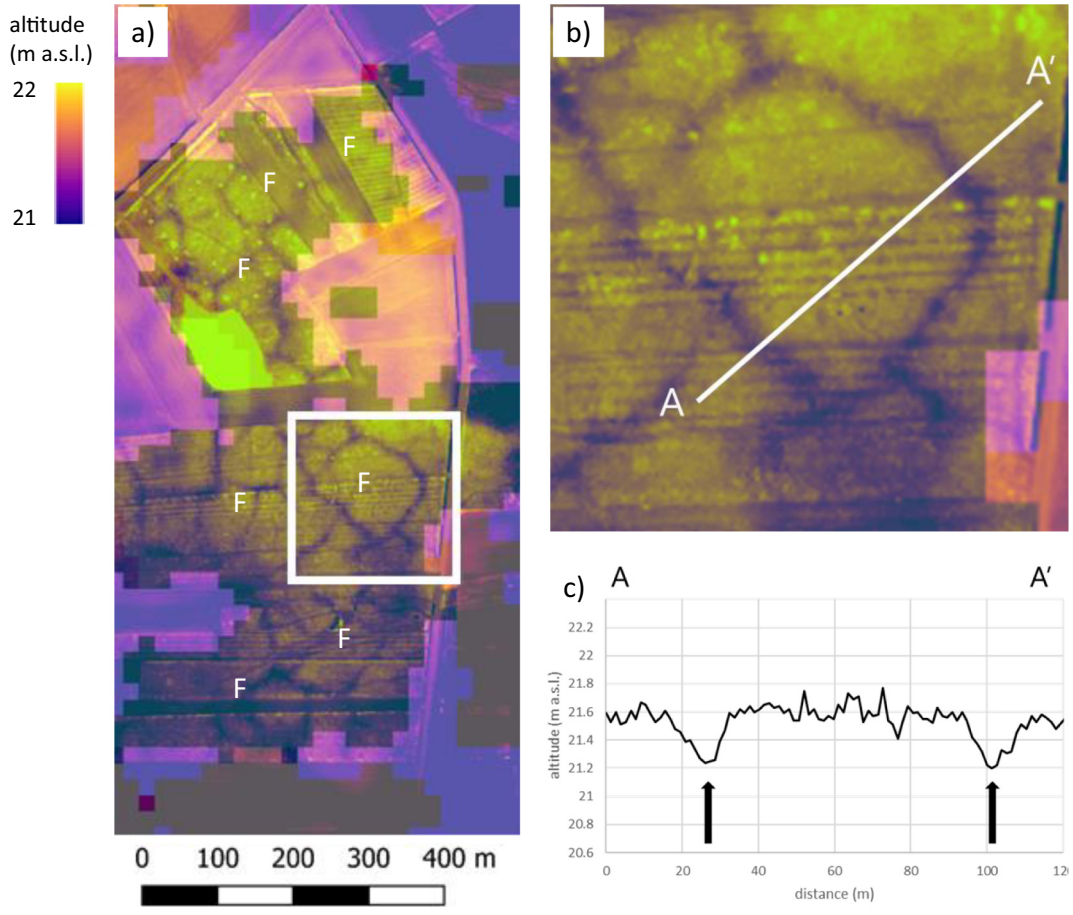

Fig. 4. (a) Mapped polygons at site Tikkebroeken (TB), a nature reserve in Kasterlee. Areas with forest vegetation are indicated with 'F' – it can be seen that polygon traces are clearest when observed under forest. Rectangle refers to map shown in (b). (b) The line A-A′ refers to the topographical profile shown in (c). (c) Topographical signature of polygon boundaries.

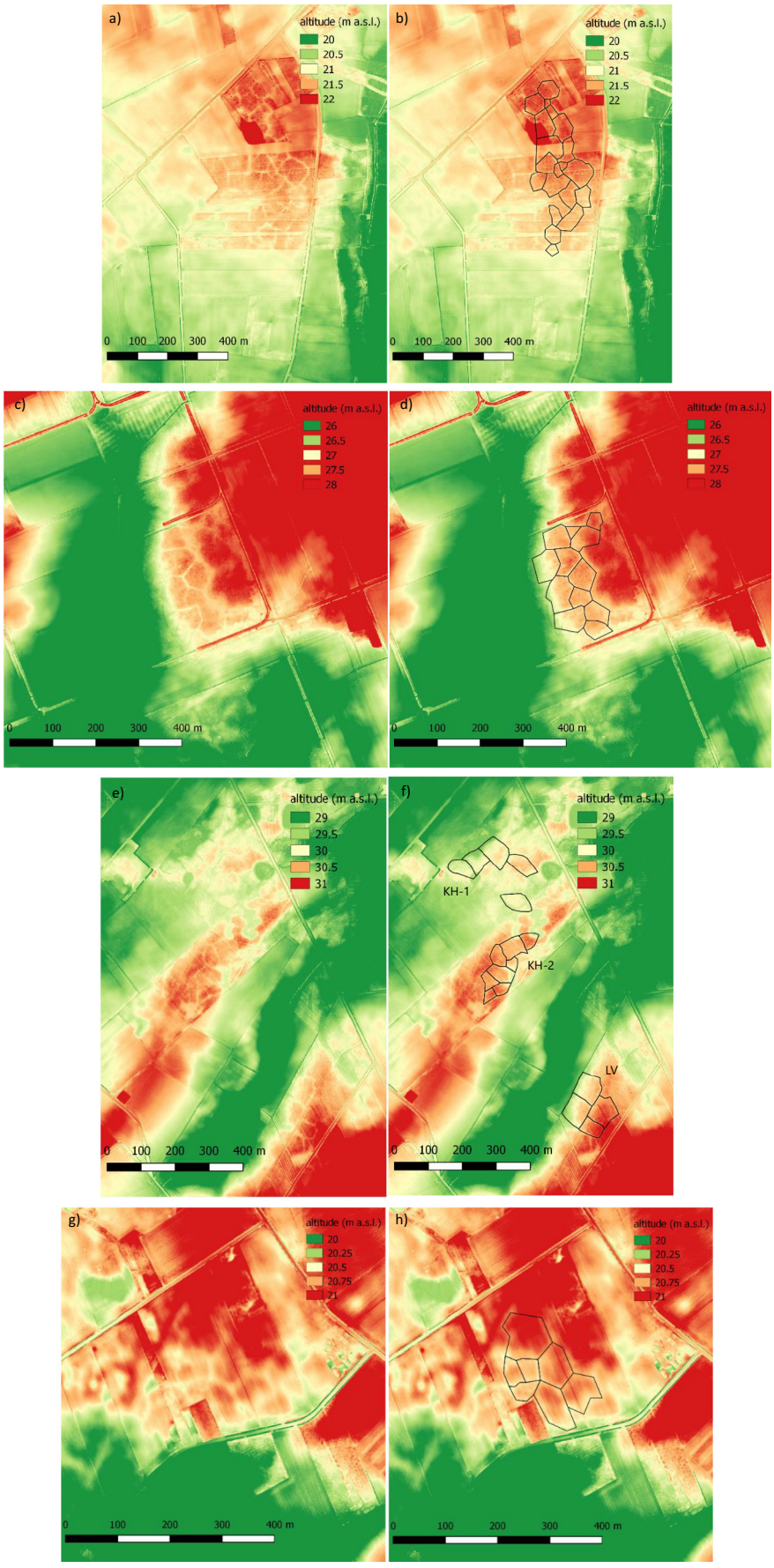

Fig. 5. (a–b) Mapped polygons at site Tikkebroeken (TB). (c–d) Mapped polygons at site Liereman (LM). (e–f) Mapped polygons at sites Koevenheide (KV) and Langvenheide (LV). (g–h) Mapped polygons at site Grote Reesdijk.

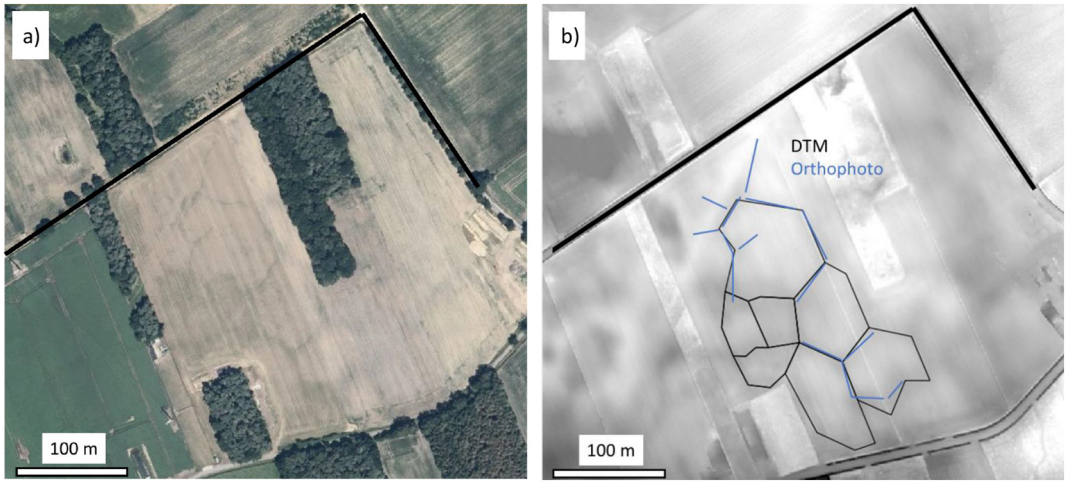

Fig. 6. Cropmarks at site Grote Reesdijk. (a) Mid-scale coloured orthophoto (Geopunt, 2015). (b) Comparison between cropmarks (blue lines) and the DEM image (black lines).

m^2 (site SB-3). Some networks are regular, at least in terms of the RSD, which may be as small as 16% (site KV). The highest RSD is observed for site Mellen (59%). Any relative number for ORTHO and 4RAY can be observed, and overall ranges between 0% and 100%. Polygon networks that are located on the Campine Clay cuesta, and are underlain by the clayey Weelde Formation, seem to display a wide range for MEAN and ORTHO and a smaller RSD (networks SB, KV, KH, LV, LM; Fig. 7a; category 1). Networks that are not underlain by the Weelde Formation, and are situated on the Brasschaat pediment, systematically show a large RSD for the mean polygon area (networks DV, ME, TB, GR; Fig. 7a, category 2). This is also reflected in the RSD plot for categories related to the depth of the clay (Fig. 7b, category 4 and 5). The clearest relation of polygon characteristics with the local geomorphological setting is seen for ORTHO (Fig. 7c). The percentage is, on average, lowest for sites that are situated on a crest (networks SB-3, KV, KH-1, KH-2; Fig. 7c, category 4). Next, a clear relation is present between the present-day soil drainage class and RSD, 4RAY and ORTHO. Networks that developed in soils that are indicated as wet today (Fig. 7d; category 2) show smaller values for RSD, 4RAY and ORTHO (networks KV, KH-1, KH-2, LV, LM). The network classification was also checked against network characteristics (Fig. 7e). Here it can be seen that regular hexagonal (KV; category 1) and orthogonal (SB-1, LV; category 5) networks show the largest MEAN and smallest RSD. Overall, the percentage 4RAY and ORTHO gradually rises for networks that were classified with a significant orthogonal component (Fig. 7e, category 4 and 5).

These observations can be summarized as follows (Fig. 7). Sites that are located in a wetter landscape have favored the development of networks that show less variation in polygon size (MEAN) and a low percentage of orthogonal intersections (ORTHO, Fig. 7d). Such sites are characterised by a shallow clay layer (Fig. 7a) and are positioned on the Campine Clay cuesta. Furthermore, the percentage of ORTHO seems to be lowest for sites that are located on a local topographical crest, even though the altitude difference between crest and surrounding landscape is only 1–2 m (Fig. 7c). There seems to be a preference for

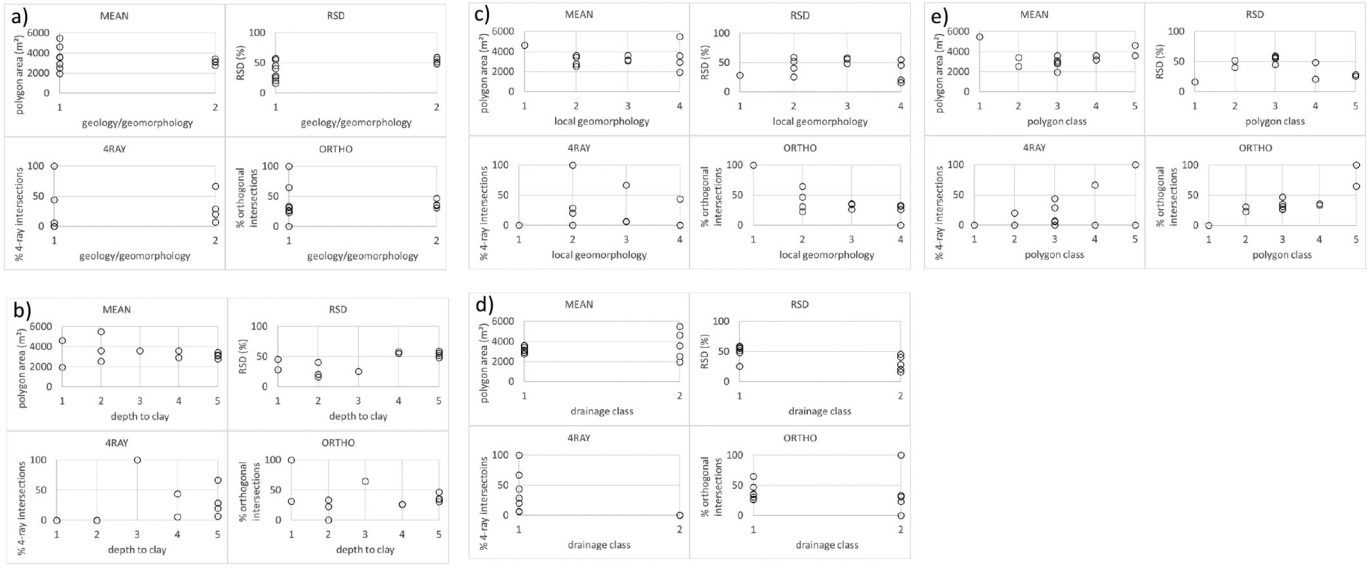

Fig. 7. (a) Polygon network characteristics (MEAN, RSD, 4RAY and ORTHO) according to the major geological/geomorphological position. 1 = underlain by Weelde Formation (Campine Clay cuesta); 2 = not underlain by Weelde Formation (Brasschaat Pediment). (b) Polygon network characteristics (MEAN, RSD, 4RAY and ORTHO) according to the depth of the first significant subsurface clay layer. 1 = 0–2 m; 2 = 2–5 m; 3 = 5–10 m; 4 = >10 m; 5 = >100 m. (c) Polygon network characteristics (MEAN, RSD, 4RAY and ORTHO) according to the local geomorphological setting. 1 = smooth dipping valley border; 2 = smooth flat valley border; 3 = undulating valley border; 4 = undulating crest. (d) Polygon network characteristics (MEAN, RSD, 4RAY and ORTHO) according to the present-day soil drainage class. 1 = moderately dry to moderately wet; 2 = moderately wet to wet. (e) Polygon network characteristics (MEAN, RSD, 4RAY and ORTHO) according to the polygon classification. 1 = hexagonal; 2 = random hexagonal/orthogonal; 3 = random mixed; 4 = random orthogonal/hexagonal; 5 = orthogonal.

orthogonal networks to develop in a valley border setting. Finally, almost pure orthogonal and hexagonal networks show the largest MEAN and the smallest RSD (Fig. 7e).

5.4. Ground Penetrating Radar profiling

Ground Penetrating Radar (GPR) can be used to image ice-wedge casts or relict sand wedges in the subsoil (Verbeeck et al., 2017). Therefore, this technique was tested to verify the existence of subsoil anomalies underneath supposed polygon boundaries. In total 35 lines were acquired, but only five of them will be shown and discussed here. The other GPR profiles did not reveal any subsoil disturbances, which is probably due to the weak contrast in dielectric properties between host and wedge material.

The first site that was imaged with GPR is Tikkebroeken (TB, line 257; Fig. 8a). The corresponding image is shown in Fig. 8d. This profile, as it was acquired with the higher-frequency 250 MHz antenna, has a limited penetration and shows strong attenuation below ca. 2 m depth. Reflections below this depth (mimicking the surface reflection) are regarded as artefacts. An interesting observation is the shallow disturbance (0–1 m depth) around the centre of the polygon trough (depression; green arrow). However, it should be noted that 5–10 m to the east and west similar disturbances are present (blue circles), without any traces in the topography. In summary, the GPR survey at this site did not produce convincing evidence for the presence of an ice-wedge cast or relict sand wedge. Line 291 (Fig. 8e) originates from the Koevenheide site (Fig. 8b). Some disturbances can be seen between a depth of 1–2 m (blue circle), near the centre of the inter-polygon trough. Remarkably, some shallow layers seem to be pushed upwards. However, a clear wedge structure cannot be observed. Line 298 (Fig. 8f) originates from the Liereman site (Fig. 8c) and shows clear disturbances (bounded by two blue lines) around the position of the polygon trough (green arrow indicates the centre of the depression). In the shallow subsurface (around 0.5 m depth) a strong saucer-shaped reflection is observed near the centre of the through, which is intercalated between undisturbed reflections above and below, and disappears to the left and right. Around 1 m depth, and again around 3 m depth, the stratification seems to be disturbed where the presence of a buried ice-wedge cast (or relict sand wedge) is assumed. Lines 300 (Fig. 8g) and 301 (Fig. 8h) were also shot at the Liereman site (Fig. 8c) and show some disturbance in the region of the trough, but less clear than in the profile corresponding to line 298. Line 301 shows a similar intercalated reflection as in line 298, which is missing outside the assumed wedge boundaries. In summary, identifying wedge structures with GPR is not straightforward at the investigated sites. A possible explanation can be the weak dielectric contrast between host and wedge material, certainly for site TB. Alternatively, the measurement conditions in saturated soil may not have been optimal. In at least one profile (site LM, line 298), there are strong arguments in favor of a wedge structure in the subsurface. This site is proven to have a shallow clay layer in the subsurface.

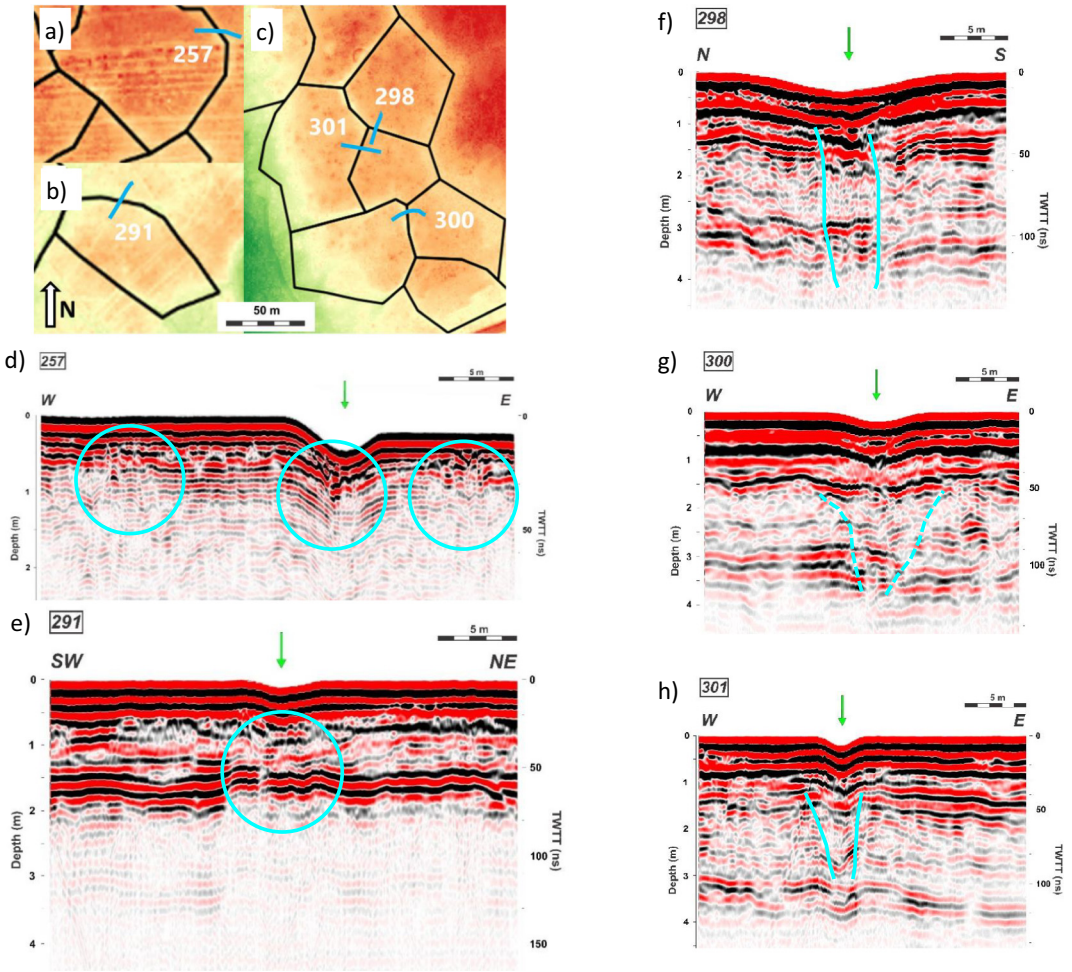

Fig. 8. (a) Location of GPR line 257 (TB). (b) Location of GPR line 291 (KH−1). (c) Location of GPR lines 298, 300 and 301 (LM). (d) GPR profile 257, Tikkebroeken (TB); green arrow indicates the position of the centre of the topographic depression; blue circles indicate (weak) disturbances in the subsoil. (e) GPR profile 291, Koevenheide (KH-1); green arrow indicates the position of the centre of the topographic depression; blue circle indicates disturbances in the subsoil as the layers seem to be pushed upward slightly. (f, g, h) GPR profiles 298, 300, 301, Liereman (LM); green arrows indicates the position of the centre of the topographic depression; blue lines bound the suggested wedge structures.

6. Discussion

The polygon networks as observed on LiDAR DEM (resolution 1 m^2) undoubtedly represent thermal contraction crack polygons formed during one or several episodes of permafrost development (Figs. 4, 5 and 6). Desiccation cracking might produce (very) large polygon patterns as well, but this process is not considered to be relevant in sandy soil (El Maarry et al., 2012).

As the polygon boundaries are expressed as shallow depressions, several 10 cm deep and several meter wide (up to 10 m), it can be advocated that they are the surface expression of relict ice-wedges. Present-day polygon boundaries of active cracks in permafrost regions are usually expressed as a pronounced shoulder-trough-shoulder topography which is reorganized after melting of the permafrost and subsequent collapsing of the wedge into a flat shoulder-trough-flat shoulder topography. Melting of ice-wedges would produce variation in topography while sand-wedges would not, because there is ice involved in developing the former, leaving a cavity that is being filled only partly (immediately or later on). GPR imaging of polygon boundaries in the Campine only provides convincing evidence of subsoil disturbances underneath the troughs at the Liereman site (Fig. 8). However, the weak difference in dielectric properties between host material (sand) and infill (sand) at some locations may be a limiting factor in the usefulness of GPR imaging for this purpose. Yet, in any case the layering should at least be disturbed underneath the troughs, which indeed can be observed on several GPR images.

The internal morphometric analysis, i.e., the comparison of Campine polygon networks against geomorphological, geological, pedological and hydrological parameters did reveal some interesting relationships (Fig. 7). As indicated above, networks that are located on the Campine Clay cuesta with a clay layer in the shallow subsoil are slightly better organized (see lower RSD in Fig. 7a for category 1 and in Fig. 7b for categories 1-2-3). This might suggest that they are in a slightly later stage of development. However, if so, these networks should also have a smaller mean polygon size, which cannot be observed from Fig. 7a. As such, the relationship is non-existing or remains unclear. Whether they are located on the cuesta or not, some networks are orthogonal and well-organized, a characteristic that might be inferred from the percentage of orthogonal intersections and the relative standard deviation of the mean polygon area (e.g., SB-1 and LV; Table 4). Very interestingly, these networks are located close to a valley border (Fig. 5c–d; Fig. S1d). Indeed, Mackay (1999) already pointed out that orthogonal networks usually develop on heterogeneous terrain, close to a scarp or when a surface is drying out. These networks thus seem to have been developing on a surface bounded by a slope adjacent to the valley floor which is only 1–2 m lower. Other networks, like TB, GR, ML and DV are more chaotic and complex and probably developed further away from emerging valley borders. Site LM (Fig. 5k–l) also developed close to a valley border, however, the network has a strong hexagonal component.

The average fossil polygon size in the Campine area is ca. 3000 m^2, as determined from LiDAR DEM images. An average polygon size of ca. 3000 m^2 would correspond to hypothetical orthogonal polygons of 50 m by 60 m. Crack spacings of this magnitude have sometimes been observed in long geological cross-sections. Kasse and Vandenberghe (1998) observed crack spacings of up to 50 m and more near the Dutch-German border and Verbeeck et al. (2017) observed two ice-wedge casts in a palaeoseismological trench in northeastern Belgium spaced ca. 70 m. It should be noted that the apparent crack spacing from long geological cross-sections is obviously dependent on the orientation of the cross-section relative to the polygon boundary.

The size difference of the Campine polygons with present-day, analogues is striking (Fig. 7). A mean polygon size of ca. 3000 m^2 is much more than that for any of the investigated analogues (Table 2). Nevertheless, the present-day analogue that most closely matches the Campine networks is found at Adventdalen (Svalbard, Norway), most notably the inactive networks from the upper Adventdalen, which appear to be rather large (Ulrich et al., 2011). Furthermore, the largest polygon size at Adventdalen (network AD2 with an average polygon size of 3329 m^2) approximates the mean value of the fossil Campine networks (Tables 2 and 4). This may suggest that some of the Adventdalen polygons, the largest ones, did not evolve into a more mature stage (i.e., more subdivision), as a result of less favourable conditions (e.g., higher ground temperatures; Ulrich et al., 2011). As such, these may be good analogues for the Campine polygons. In this context, it is also mentioned that the percentage of 4-ray intersections (4RAY) at Adventdalen, which is amongst the smallest for the listed present-day analogues, does not differ that much from the percentage 4-ray intersections in the fossil Campine networks (Table 2). All other Arctic examples have much higher percentages of 4-ray intersections, and much smaller mean (MEAN) and maximum (MAX) polygon sizes. It is probably not a coincidence that these are all located in areas with a lower MAAT. Unfortunately, the dataset of the modern examples is too small to perform a statistical analysis. Furthermore, apart from temperature, other factors such as time will play a major role in the determination of polygon size and shape. As indicated in Section 3, the maximum amount of available time during which the Adventdalen polygons could develop is ca. 10 kyr. Consequently, if we accept the Adventdalen sites as suitable analogues, this amount of time could serve as a maximum estimate for the time needed to develop the Campine polygons.

However, it should be noted that the geographical setting of Svalbard is completely different than for Late Weichselian western Europe. Adventdalen is located on an island, in a coastal setting surrounded by an ice-free ocean (Gulf stream), while the Campine area was situated in a more continental setting at that time. In addition, Svalbard is located north of the Arctic Circle, where the seasonal periodicity of daylight and darkness favours longer and more severe cycles and deeper ground freezing (Lowe and Walker, 1997), as opposed to the mid-latitude Campine area where diurnal freeze-thaw cycles are more dominant. Even though fossil periglacial phenomena seem useful to identify past cold environments, caution should be taken when using this type of evidence in palaeoclimatic reconstructions (Ballantyne and Harris, 1994; Lowe and Walker, 1997).

Next, it remains to be confirmed whether the present-day surface features in the Campine area, as observed on LiDAR DEM, are representative for the entire polygon networks and their full extent and stage of development. Smaller wedges might have developed, producing 2nd and 3rd order polygons, which may be too small to leave a surface expression, or may be obliterated by later surface processes. Some of the wedge casts described by Ghysels (2008) are probably good examples of small higher order cracks which would not leave a topographical surface expression, even in the case of ice-wedges. However, they may still be visible as cropmarks and this might be a reason why the average polygon size in Flanders, as determined from cropmarks (Ghysels, 2008), is (much) smaller than that from the Campine area.

As indicated above, the average polygon dimension of the Campine networks is very large, which suggests that they represent a first order network. Furthermore, this first order network is thought to represent a relict ice-wedge network, instead of a sand-wedge network. The topographic expression of the first order networks in the Campine is indicative of subsoil volume loss during ice-rich permafrost melting, given the rather deep inter-polygon throughs, as already explained above (Fig. 4c). Relict sand-wedges would not produce significant topography. The only two sites where cropmarks were observed, Kijkverdriet (KV) and Grote Reesdijk (GR) (Fig. 6), reveal that these cropmarks do not increase the complexity of the LiDAR-based polygon network interpretation. It thus remains questionable whether a 2nd and/or 3rd order network developed, because these would have left traces in the form of vegetation marks as well.

Fossil irregular networks with large polygons have been observed elsewhere in Europe, notably in France (see Fig. 1B in Bertran et al., 2013) and Poland (network type A in Ewertowski et al., 2017). They were most likely formed during the Late Weichselian (Late Pleniglacial) but the exact duration of development is not known. On the contrary,

very small polygon networks are also known from France (Andrieux et al., 2016) and the western part of Flanders (Ghysels, 2008). The available dating evidence suggests a Late Pleniglacial age for these networks. The reason for the large size discrepancy between the Campine polygons and the fossil polygons in France and the western part of Flanders is not clear yet. One possible explanation may include the method of detection. Polygons from the French and western Flanders analogues were mapped using satellite and orthophoto imagery, which means that networks are identified based on cropmarks or lineations in grassland, and possibly also weak differences in soil properties and soil moisture. The Campine polygons are mapped using a completely different approach, i.e. a LiDAR-based digital elevation model. Possibly, only the largest ice-wedges, those that would develop as a first order network, would leave traces in the topography.

In the absence of direct age control on polygon development in the Campine region, we tentatively correlate the networks studied here with those in the western part of Flanders. There, the relict sand and composite wedges are dated between 22 ka and 14 ka, i.e., the Late Weichselian stage (Ghysels, 2008). This time window of ca. 8 kyr is in agreement with, e.g., the duration of polygon development on Svalbard during the Holocene (maximum 10 kyr, and probably even less given the fact that the early Holocene in Svalbard was up to 7 °C warmer than today; van der Bilt et al., 2019). The cold period shortly after 20 ka BP as shown in the Weichselian temperature reconstruction in Fig. 3, falls within this time window. The proposed time window is also in agreement with recent recharge age estimates for the Ledo-Paniselian aquifer (Walraevens et al., 2020), which show a clear gap in modelled radiocarbon ages between 20 ka and 14 ka. This may well be explained by the development of permafrost, probably continuous, which causes the disconnection of surface water and groundwater, as such preventing recharge. Likely, if polygon networks were to develop, this period of (dis) continuous permafrost would be a good candidate. Alternatively, the recharge gap may have been caused by limited availability of infiltrating water due to the relatively arid climate (Kasse, 2002). Yet, soils would have been sufficiently wet as to allow the development of ice-wedges.

7. Conclusion

LiDAR revealed the existence of relict periglacial polygons in the Campine area. They are usually preserved in woodlands and heathlands where orthophotos yield no information. The polygons are interpreted as ice-wedge casts formed in a permafrost environment, as a result of thermal contraction cracking, probably during the Late Weichselian. Cropmarks could only be observed at two sites, and do not differ significantly from the LiDAR images. Campine polygons are generally poorly subdivided and larger than any other present-day arctic example. Some of the Holocene polygon networks at Svalbard may nevertheless be suitable analogues, although it has to be born in mind that solar dynamics would have been different during the Late Weichselian in western Europe. The large polygons observed in the Campine area probably reflect a period of a few thousands of years of ice-wedge development in sufficiently wet soils. The features that are captured by the LiDAR DEM probably reflect a first order network. However, it cannot be ruled out that smaller 2nd and 3rd order polygons remained undetected on the LiDAR images, as they may have been erased by subsequent surface processes or were too small to leave a topographical trace. GPR measurements provide some evidence of subsoil disturbances below polygon boundaries where relict ice-wedge casts are expected. The most obvious images are from the Liereman site (LM) – consequently, this site is being put forward as a candidate site for trenching which is believed to be the ultimate verification tool. Since many factors contribute to the final shape and size of individual polygons in present-day and fossil networks, identifying and isolating driving forces such as time and temperature is not straightforward.

Supplementary data to this article can be found online at https://doi.org/10.1016/j.geomorph.2020.107582.

Declaration of competing interest

The authors declare that they have no known competing financial interests or personal relationships that could have appeared to influence the work reported in this paper.

Acknowledgements

This work is performed in close cooperation with, and with the financial support of NIRAS/ONDRAF, the Belgian Agency for Radioactive Waste and Fissile Materials, as part of the programme on geological disposal of high-level/long-lived radioactive waste that is carried out by ONDRAF/NIRAS.

References

Abolt, C.J., Young, M.H., Caldwell, T.G., 2017. Numerical modelling of ice-wedge polygon geomorphic transition. Permafr. Periglac. Process. 28, 347–355.
AGIV, 2014. Digitaal Hoogtemodel Vlaanderen II, DEM, Raster, 1 m.
Andrieux, E., Bertran, P., Saito, K., 2016. Spatial analysis of he French Pleistocene permafrost by a GIS database. Permafr. Periglac. Process. 27, 17–30.
Ballantyne, C.K., Harris, C., 1994. The Periglaciation of Great Britain. Cambridge University Press, Cambridge.
Beerten, K., Verbeeck, K., Laloy, E., Vanacker, V., Vandenberghe, D., Christl, M., De Grave, J., Wouters, L., 2020. Electron spin resonance (ESR), optically stimulated luminescence (OSL) and terrestrial cosmogenic radionuclide (TCN) dating of quartz from a Plio-Pleistocene sandy formation in the Campine area, NE Belgium. Quat. Int. 556, 144–158.
Bertran, P., Andrieux, E., Antoine, P., Coutard, S., Deschodt, L., Gardère, P., Hernandez, M., Legentil, C., Lenoble, A., Liard, M., Mercier, N., Moine, O., Sitzia, L., Van Vliet-Lanoë, B., 2013. Distribution and chronology of Pleistocene permafrost features in France: database and first results. Boreas 43, 699–711.
van der Bilt, W.G.M., D'Andrea, W.J., Werner, J.P., Bakke, J., 2019. Early Holocene temperature oscillations exceed amplitude of observed and projected warming in Svalbard lakes. Geophys. Res. Lett. 24, 14732–14741.
Burn, C.R., O'Neill, H.B., 2015. Subdivision of ice-wedge polygons, western Arctic coast. 7th Canadian Permafrost Conference, at Quebec City.
Busschers, F.S., Kasse, C., van Balen, R.T., Vandenberghe, J., Cohen, K.M., Weerts, H.J.T., Wallinga, J., Johns, C., Cleveringa, P., Bunnik, F.P.M., 2007. Late Pleistocene evolution of the Rhine-Meuse system in the southern North Sea basin: imprints of climate change, sea-level oscillation and glacio-isostacy. Quat. Sci. Rev. 26, 3216–3248.
Buylaert, J.P., Ghysels, G., Murray, A.S., Thomsen, K.J., Vandenberghe, D., De Corte, F., Heyse, I., Van den Haute, P., 2009. Optical dating of relict sand wedges and composite-wedge pseudomorphs in Flanders, Belgium. Boreas 38, 160–175.
Dafflon, B., Hubbard, S., Ulrich, C., Peterson, J., Wu, Y., Wainwright, H., Kneafsey, T.J., 2016. Geophysical estimation of shallow permafrost distribution and properties in an ice-wedge polygon-dominated Arctic tundra region. Geophys. 81, WA247–WA263.
De Gans, W., 1983. Fossiele permafrostverschijnselen in Nederland. Grondboor Hamer 6, 175–184.
De Moor, G., Pissart, A., 1992. Het reliëf. In: Denis, J. (Ed.), Geografie van België. Gemeentekrediet, Brussel, pp. 129–215.
El Maarry, M.R., Kodikara, J., Wijessoriya, S., Markiewicz, W.J., Thomas, N., 2012. Desiccation mechanism for formation of giant polygons on Earth and intermediate-sized polygons on Mars: results from a pre-fracture model. Earth Planet. Sci. Lett. 323-324, 19–26.
Ewertowski, M., Kijowski, A., Szuman-Kalita, I., Tomczyk, A., Kasprzak, L., 2017. Low-altitude remote sensing and GIS-based analysis of cropmarks: classification of past thermal-contraction-crack polygons in central western Poland. Geomorphol. 293, 418–432.
Farnsworth, W.R., Allaart, L., Ingólfssond, O., Alexanderson, H., Forwick, M., Noormets, R., Retelle, M., Schomacker, A., 2020. Holocene glacial history of Svalbard: Status, perspectives and challenges. Earth Sci. Rev. 208, 103249.
French, H.M., 2007. The Periglacial Environment. third ed. John Wiley & Sons, Chichester, UK.
Geopunt, 2013. Geologisch 3D lagenmodel van Vlaanderen en het Brussels Hoofdstedelijk Gewest, versie 2 (G3Dv2) (accessed 2018-04-02).
Geopunt, 2015. Orthofotomozaïek, middenschalig, zomeropnamen, 2015. Vlaanderen. (Accessed 20 March 2018).
Geopunt, 2017. Digitale bodemkaart van het Vlaams Gewest: bodemtypes, substraten, fasen en varianten van het moedermateriaal en de profielontwikkeling. WRB Soil Units 40k: Bodemkaart van het Vlaamse Gewest volgens het internationale bodemclassificatiesysteem World Reference Base op schaal 1:40.000 (accessed 2018-04-02).
Ghysels, G., 2008. Bijdrage tot de studie van de kenmerken, de genese en de datering van periglaciale polygonale wigstructuren in België. (PhD-thesis). Ghent University.
Ghysels, G., Heyse, I., 2006. Composite-wedge Pseudomorphs in Flanders, Belgium. Permafr. Periglac. Process. 17, 145–161.
van Gijssel, K., 1995. A hydrogeological and palaeoenvironmental data set for large-scale groundwater flow model simulations in the northeastern Netherlands. Meded. Rijks Geol. Dienst 52, 105–134.
Govaerts, J., Beerten, K., ten Veen, J., 2016. Weichselian permafrost depth in the Netherlands: a comprehensive uncertainty and sensitivity analysis. Cryosph. 10, 2907–2922.

Gullentops, F., Paulissen, E., Vandenberghe, J., 1981. Fossil periglacial phenomena in NE Belgium (excursions in the Kempen on 26 and 27 september 1978). Biul. Periglacjalny 28, 345–365.

Haltigin, T.W., Pollard, W.H., Dutilleul, P., Osinski, G., 2012. Geometric evolution of polygonal terrain networks in the Canadian high arctic: evidence of increasing regularity over time. Permafr. Periglac. Process. 23, 178–186.

Huijzer, B., Vandenberghe, J., 1998. Climatic reconstruction of the Weichselian Pleniglacial in northwestern and central Europe. J. Quat. Sci. 13, 391–417.

Kasper, J.N., Allard, M., 2001. Late-Holocene climatic changes as detected by the growth and decay of ice wedges on the southern shore of Hudson Strait, northern Quebec, Canada. The Holocene 11, 563–577.

Kasse, C., 2002. Sandy aeolian deposits and environments and their relation to climate during the Last Glacial Maximum and Lateglacial in northwest and central Europe. Prog. Phys. Geogr. 26, 507–532.

Kasse, C., Vandenberghe, J., 1998. Topographic and drainage control on Weichselian ice-wedge and sand-wedge formation, Vennebrügge, German-Dutch border. Permafr. Periglac. Process. 9, 95–106.

Kasse, C., Vandenberghe, D., De Corte, F., Van den Haute, P., 2007. Late Weichselian fluvio-aeolian sands and coversands of the type locality Grubbenvorst (southern Netherlands): sedimentary environments, climate record and age. J. Quat. Sci. 22, 695–708.

Kokelj, S.V., Pisaric, M.F.J., Burn, C.R., 2007. Cessation of ice-wedge development during the 20th century in spruce forests of eastern Mackenzie Delta, Northwest Territories, Canada. Can. J. Earth Sci. 44, 1503–1515.

Lachenbruch, A.H., 1962. Mechanics of thermal contraction cracks and ice-wedge polygons in permafrost. Spec. Pap. Geol. Soc. Am. 70 (69 p.).

Lachenbruch, A.H., 1966. Contraction theory of ice-wedge polygons: a qualitative discussion. Proc. Permafrost Int. Conf., Lafayette, Indiana. Publ., 1287. U.S. Natl. Acad. Sci, Washington, D. C, pp. 63–71.

Long, A.J., Strzelecki, M.C., Lloyd, J.M., Bryant, C.L., 2012. Dating High Arctic Holocene relative sea level changes using juvenile articulated marine shells in raised beaches. Quat. Sci. Rev. 48, 61–66.

Lowe, J.J., Walker, M.J.C., 1997. Reconstructing Quaternary Environments. second ed. Addison Wesley Longman Limited.

Mackay, J.R., 1999. Periglacial features developed on the exposed lake bottoms of seven Lakes that drained rapidly after 1950, Tuktoyaktuk Peninsula Area, Western Arctic Coast, Canada. Permafr. Periglac. Process. 10, 39–63.

Murton, J.B., Kolstrup, E., 2003. Ice-wedge casts as indicators of palaeotemperatures: precise proxy or wishful thinking? Prog. Phys. Geogr. 27, 155–170.

NGRIP – North Greenland Ice Core Project members, 2004. High-resolution record of Northern Hemisphere climate extending into the last interglacial period. Nat. 431, 147–151.

Plug, L.J., Werner, B.T., 2001. Fracture networks in frozen ground. J. Geophys. Res. 106, 8599–8613.

Renssen, H., Vandenberghe, J., 2003. Investigation of the relationship between permafrost distribution in NW Europe and extensive winter sea-ice cover in the North Atlantic Ocean during the cold phases of the Last Glaciation. Quat. Sci. Rev. 22, 209–223.

Romanovskii, N.N., 1985. Distribution of recently active ice and soil wedges in the USSR. In: Church, M., Slaymaker, O. (Eds.), Field and Theory; Lectures in Geocryology. University of British Columbia Press, Vancouver, pp. 154–165.

Sletten, R.S., Hallet, B., Fletcher, R.C., 2003. Resurfacing time of terrestrial surfaces by the formation and maturation of polygonal patterned ground. J. Geophys. Res. 108 (E4), 8044.

Ulrich, M., Hauber, E., Herzschuh, U., Härtel, S., Schirrmeister, L., 2011. Polygon pattern geomorphometry on Svalbard (Norway) and western Utopia Planitia (Mars) using high-resolution stereo remote-sensing data. Geomorph. 134, 197–216.

Vandenberghe, J., 1983. Some Periglacial Phenomena and their Stratigraphical Position in Weichselian Deposits in the Netherlands. Polarfurschung 53, 97–107.

Vandenberghe, J., Pissart, A., 1993. Permafrost changes in Europe during the Last Glacial. Permafr. Perigl. Proc. 4, 121–135.

Vandenberghe, J., French, H.M., Gorbunov, A., Marchenko, S., Velichko, A.A., Jin, H., Cui, Z., Zhang, T., Wan, X., 2014. The Last Permafrost Maximum (LPM) map of the Northern Hemisphere: permafrost extent and mean annual air temperatures, 25–17 ka BP. Boreas 43, 652–666.

Verbeeck, K., Wouters, L., Vanneste, K., Camelbeeck, T., Vandenberghe, D., Beerten, K., Rogiers, B., Schiltz, M., Burow, C., Mees, P., De Grave, J., Vandenberghe, N., 2017. Episodic activity of a dormant fault in tectonically stable Europe: the Rauw fault (NE Belgium). Tectonophys. 699, 146–163.

Vernes, R.W., Deckers, J., Bakker, M.A.J., Bogemans, F., De Ceukelaire, M., Doornenbal, J.C., den Dulk, M., Dusar, M., Van Haren, T.F.M., Heyvaert, V.M.A., Kiden, P., Kruisselbrink, A.F., Lanckacker, T., Menkovic, A., Meyvis, B., Munsterman, D.K., Reindersma, R., Rombaut, B., ten Veen, J.H., van de Ven, T.J.M., Walstra, J., Witmans, N., 2018. Geologisch en hydrogeologisch 3D model van het Cenozoïcum van de Belgisch-Nederlandse grensstreek van Midden-Brabant/De Kempen (H3O – De Kempen). TNO-rapport, in opdracht van Vlaams Planbureau voor Omgeving, Vlaamse Milieumaatschappij, TNO Geologische Dienst Nederland, Nederlandse Provincie Noord-Brabant, Brabant Water, Programmabureau KRW/DHZ Maasregio (109 pp.).

Walraevens, K., Blaser, P., Aeschbach, W., Van Camp, M., 2020. A palaeoclimatic record from the Ledo-Paniselian Aquifer in Belgium – indications for groundwater recharge and flow in a periglacial environment. Quat. Int. 547, 127–144.